Preparation, Characterisation and Performance of Encapsulated Copper–Ruthenium Bimetallic Catalysts Derived from Molecular Cluster Carbonyl Precursors

Douglas S. Shephard, Thomas Maschmeyer, Gopinathan Sankar, John Meurig Thomas,* Dogan Ozkaya, Brian F. G. Johnson,* Robert Raja, Richard D. Oldroyd, and Robert G. Bell

Abstract: The advantages of producing high-performance, bimetallic nanoparticle catalysts from their precursor metal-cluster carbonylates anchored inside the mesoporous channels of silica (MCM41) are described. In situ X-ray absorption and FT-IR spectroscopies as well as ex situ high-resolution scanning transmission electron microscopy were used to chart the progressive conversion, by gentle thermolysis, of the parent carbonylates to the denuded, bimetallic nanoparticle catalysts. Separate copper and ruthenium K-edge X-ray absorption spectra yield a detailed structural picture of the active, approximately 15 Å diameter catalyst: it is a rosette-shaped entity in which twelve exposed Ru atoms are connected to a square base composed of relatively concealed Cu atoms. These in turn are anchored by four oxygen bridges to four Si atoms of the mesopore lining. The bimetallic catalysts exhibit no tendency to sinter, aggregate or fragment into their component metals during use. The nanoparticles perform well in the catalytic hydrogenation of hex-1-ene—a detailed kinetic study at 373 K and 20 bar H_2 is presented here (maximum TOF in $[(\mathrm{mol_{substr}})(\mathrm{mol_{cluster}})^{-1}\,\mathrm{h}^{-1}]$ 51 200, average TOF 22 400)—and also in the hydrogenations at 65 bar H_2 and 373 K of diphenylacetylene, phenylacetylene, stilbene, *cis*-cyclooctene and D-limonene, the average TOFs being 17, 610, 70, 150 and 360, respectively.

Keywords: bimetallic nanoparticles · clusters · copper · heterogeneous catalysis · hydrogenations · ruthenium

Introduction

With the advent of mesoporous materials, the science and catalytic potential of oxide supports (especially siliceous ones) has undergone a revolution.[1–3] These silicas, the surface areas of which often exceed 1000 $m^2 g^{-1}$, possess a highly regular structure composed of channels the diameter of which may be controllably arranged to fall within the range 15 to 80 Å (Figure 1). The larger pore sizes of these silicas (lined with pendant silanol groups), in contrast to the smaller ones of high-silica faujasitic[4] and UTD-1[5, 6] zeolites or metal aluminophosphates like DAF-1[7] and STA-1,[8] offer the possibility of creating isolated, catalytically active sites in a structurally well-defined manner[9–11] at the inner walls of the mesopores.

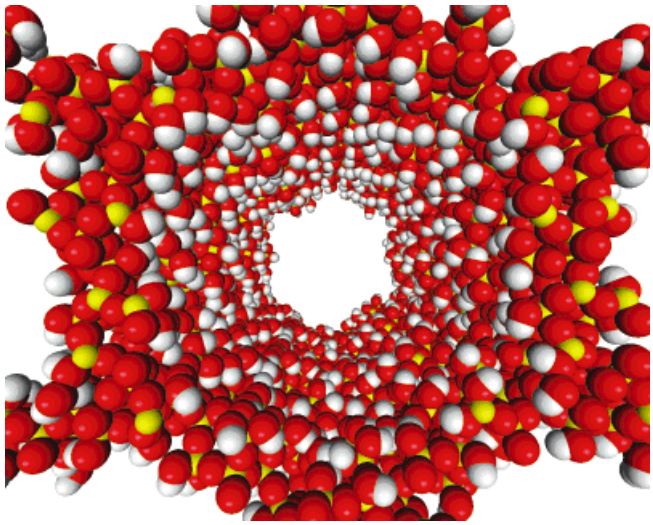

Figure 1. Computer graphic view along the axis of a single mesopore in MCM-41 silica (pore opening ≈30 Å). The profusion of pendant silanol groups lining the pore function as the anchoring points for the adsorbed species. (Colour code: yellow, silicon; red, oxygen; white, hydrogen).

[*] Prof. Sir J. M. Thomas, Dr. T. Maschmeyer, Dr. G. Sankar, Dr. R. Raja, Dr. R. D. Oldroyd, Dr. R. G. Bell
Davy Faraday Research Laboratories
The Royal Institution of Great Britain
21 Albemarle Street, London, W1X 4BS (UK)
Fax: (+44) 171-629-3569

Prof. B. F. G. Johnson, Dr. D. S. Shephard, Dr. T. Maschmeyer
The University Chemical Laboratories
Lensfield Road, Cambridge, CB2 1EW (UK)

Prof. Sir J. M. Thomas, Dr. D. Ozkaya
Department of Materials Science, University of Cambridge
New Museum Site, Cambridge, CB2 3QZ (UK)

0947-6539/98/0407-1214 $ 17.50+.50/0

Bimetallic nanoparticles themselves possess catalytic properties that differ sharply from those of solid solutions of the bulk metals. This was one of the key conclusions to emerge from the early work of Sinfelt,[12] and its veracity has been repeatedly demonstrated by subsequent workers. Among the many studies of bimetallic catalysts some are of great technological importance (e.g. Pt–Re, Pt–Ir and Pt–Rh) in processes such as the reforming of naptha and the control of auto emissions.[13] Of late, the advantages of using mixed-metal carbonyl clusters as starting materials for the production of efficient bimetallic nanoparticle catalysts have been appreciated.[14–21] For example, in Re–Ir[19] and Ag–Ru[20] systems, it is possible to follow the gradual conversion of the cluster precursor to the active catalyst using a variety of in situ (X-ray absorption and FTIR spectroscopies)[22, 23] and gravimetric techniques.

We are concentrating our discussion in this area on large carbonyl clusters in which the metals have many metal–metal connectivities since our aim is to form bimetallic particles with uniform size and composition from such a species. Hence, in our approach, we are deliberately avoiding the less readily controllable surface-mediated synthesis, which relies on the aggregation of smaller cluster precursors as exemplified by the work of, for example, Gates et al.[16, 17]

The current interest in the use of *bimetallic* catalysts is largely due to the enhanced activity and selectivity that may be achieved by two metals working synergistically. However, despite considerable effort, the preparation of these systems by metal salt deposition and subsequent calcination followed by reduction to the active low-valent species is not always reliable and has many drawbacks, the greatest of which is the lack of control over size, morphology and homogeneity of the resulting bimetallic nanoparticle. These factors and the rather random nature of the support lead to loss of selectivity and/or activity of the catalyst, thereby rendering it in many instances inefficient.

When considering the more precise route of depositing and thermolysing carbonyl clusters for the production of supported nanoparticles, several important criteria concerning the choice of bimetallic cluster precursor have to be borne in mind. First, the protective sheath surrounding the organometallic precursor must be readily removable (we find that mild thermolysis suffices). Second, to ensure a uniform distribution of the precursor over the surface of the support the ligand sheath must interact favourably with the functional groups on the surface, the solvent and the counterion. Moreover, interactions with the surface must be stronger than those involved in solvation or between the precursor species so that aggregation into small molecular crystallites and subsequent sintering on the surface is suppressed upon removal of the CO sheath. Anionic cluster carbonyl species,[24] typified by $[Ru_6C(CO)_{16}Cu_2Cl]_2[PPN]_2$ and $[Ag_3Ru_{10}C_2(CO)_{28}Cl][PPN]_2$ (PPN = bis(triphenylphosphonyl)imminium), fulfil these criteria as their interaction with the silica (MCM41) surface is of the $Si-OH^{\delta+}\cdots{}^{\delta-}O-C-M$ type[25] and intermolecular Coulombic repulsion prevents their aggregation prior to thermolysis. A representation of this approach is given in Scheme 1.

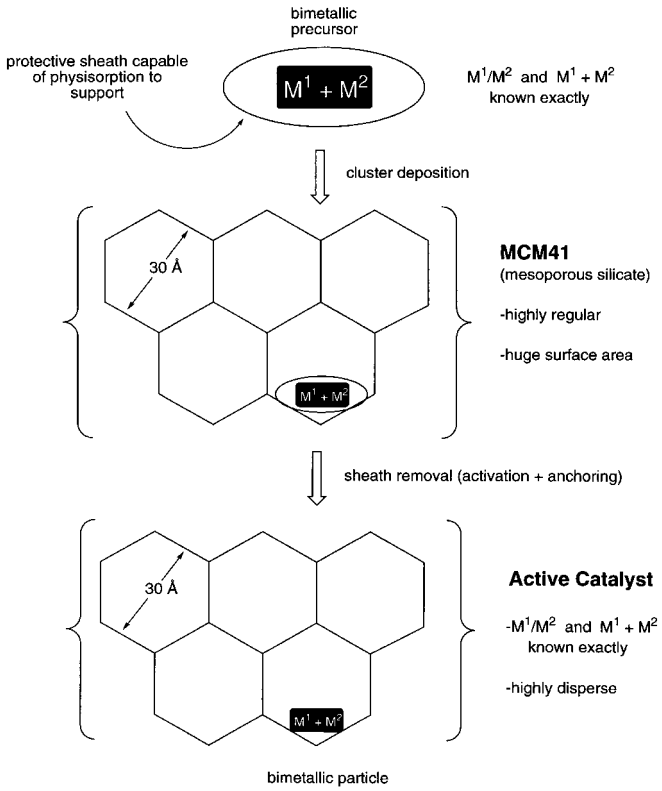

Scheme 1. The deposition and thermolysis of carbonyl clusters for the production of supported nanoparticles.

Over the last few years great progress has been made in the synthesis of large (>10 metal atoms) *bimetallic* cluster compounds of Group VIII [Fe,Ru,Os] and XI [Cu,Ag,Au] metals at the Cambridge laboratories.[24] Clusters composed of different metal ratios ($M^1/M^2 = 1$ to 4) and nuclearities ($M^1 + M^2 = 8$ to 30) have been synthesised. These anionic molecular cluster species have all been structurally characterised by single-crystal X-ray diffraction and so their precise nuclearities and metal ratios are known.

Three multicentred mixed-metal molecular cluster carbonyls that have recently been used as precursors for heterogeneous catalysts are those studied by Nasher et al.[14, 19] and Shephard et al.[20] In the former instance, where the clusters were $[PtRu_5C(CO)_{16}]$ and $[Re_6C(CO)_{18}\{\mu^3\text{-}Re(CO)_3\}\{\mu^3\text{-}Ir(CO)_2\}]^{2-}$, it was found that in the case of the Re–Ir cluster the metals segregated into separate entities upon thermolysis, possibly because of the nature of the oxide support used. In the case of the Ru–Pd cluster aggregation rather than segregation occurred, producing relatively uniform particles (reported as between 8–23 Å in size) with bimetallic composition and a fcc packing arrangment. When the cluster anion $[Ag_3Ru_{10}C_2(CO)_{28}Cl]^{2-}$ (**1**) was used,[19] there was evidence neither for segregation nor for aggregation/sintering upon thermolysis, and we believe this to be for three reasons. First, the mesoporous silica support onto which the cluster carbonylate is initially anchored is replete with silanol groups that interact strongly with the carbonylate anion. Second, the anionic character of the clusters keeps them apart during the initial stage of deposition. Third, the relative oxophilicity of the silver atoms makes them an ideal

bonding centre securing the bimetallic cluster to the oxide support.

In this paper, extending this latter philosophy, we report the detailed synthesis of the bimetallic Cu–Ru carbido carbonyl $[Ru_6C(CO)_{16}Cu_2Cl]_2[PPN]_2$ (**2**) and its adsorption onto the inner walls of well-defined[26, 27] mesoporous silica specimens known as MCM41. The resulting Cu–Ru bimetallic system is found to be potentially a more powerful heterogeneous catalyst than its Ag–Ru analogue. Apart from gaining deep insights into the nanostructures and morphology of the resulting catalysts using a combination of annular dark-field (ADF) and bright-field (BF) high-resolution scanning transmission electron microscopy,[20, 28] we tracked the precise structural details of the conversion of this precursor material into its active catalytic state principally by using the in situ X-ray absorption techniques developed at the Davy Faraday Research and Daresbury Synchrotron Radiation Laboratories.[22, 23, 29–32] We were able to gain accurate local structural information for the catalyst by the application of these element-specific techniques (i.e. for Cu and Ru). The X-ray absorption near-edge structure (XANES) investigation provides the electronic state and qualitative local structural information, whereas the extended X-ray absorption fine structure (EXAFS) study establishes the precise local structural details, thus revealing the internal structure of the nanoparticle. Confirmation of the loss of the protective carbonyl sheath during thermolysis was found by in situ FT-IR and further corroborative evidence was established by thermogravimetric analysis.

Results

Catalyst preparation: The bimetallic cluster $[Ru_6C(CO)_{16}Cu_2Cl]_2[PPN]_2$ (**2**) was synthesised by a similar, but improved, route to that described in the literature[33] in which the hexaruthenium carbido carbonylate cluster is reacted with the Cu^I salt $[Cu(MeCN)_4BF_4]$ and subsequently with bis(triphenylphosphonyl)imminium chloride (PPNCl). We found that direct reaction of an excess of CuCl in refluxing tetrahydrofuran (THF) gave better yields and was simpler to work up.

The MCM41 silica was loaded with cluster **2** by making a slurry of the two components in a mixture of ether and a small amount of a second solvent, dichloromethane (DCM), in which the cluster salt is highly soluble. This general method and solvent combination was found to be the most effective of several different preparative routes. The small amount of DCM is thought to act as a carrier, ferrying the cluster salt through the liquid phase to the silica surface, making use of entropic and enthalpic driving forces for the anions to enter the channels of the MCM41 by substitution for loosely held solvent molecules. On contact, the solvation sphere (predominantly of DCM) is substituted by the silanol-rich silica surface, allowing the diffusion of solvent molecules from the mesopores, thereby freeing them to solvate more cluster and to repeat the deposition cycle. We found this method allowed maximum dispersion (vide infra) as more conventional approaches yielded blocked pores and/or crystallites of **2**. The loading we selected for the catalysts tested here was (mol_{Salt}/mol_{MCM41}) 5:6.35 for $[Ru_{12}C_2Cu_4Cl_2(CO)_{32}][PPN]_2$/MCM41 by weight, giving rise to an approximate coverage of about one cluster per 50000 Å^2.

This catalytic precursor material was characterised by FT-IR, revealing that the carbonyl cluster was still intact. The IR spectroscopic profile of the CO stretching vibrations of the MCM41-contained clusters is considerably more complex than that of the same clusters in DCM solution (absorption maxima at 2060, 2021 and 1845 cm^{-1} for the $[Ru_{12}C_2Cu_4Cl_2(CO)_{32}]^{2-}$ cluster). Furthermore, the new absorptions (in both the terminal and bridging sections of the spectrum) show a shift to lower energy, suggesting interaction with the surface silanol groups (Figure 2). These observations

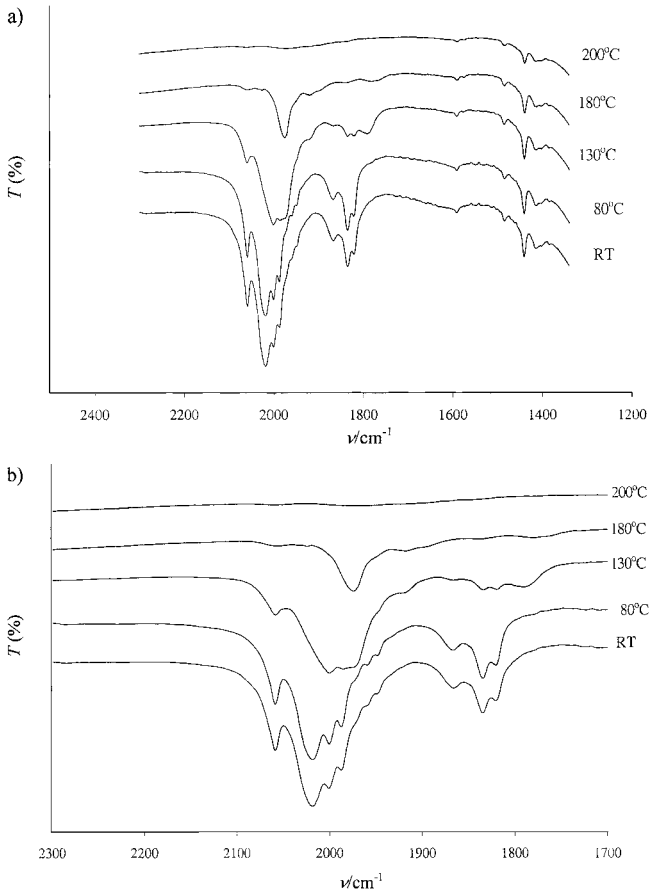

Figure 2. a) Temperature-resolved FT-IR spectra of MCM41-supported catalyst during thermolysis; b) expansion of carbonyl stretching region.

are consistent with an adsorbed $[Ru_{12}C_2Cu_4Cl_2(CO)_{32}]^{2-}$ cluster lying in a siliceous mesopore, in which both bridging and terminal COs (see crystal structure in Figure 3) are in contact with the surface. This interaction may be taken to be the dominant binding force felt by the cluster anions.[34]

In situ studies: The catalyst precursor was activated by thermolysis under high vacuum (0.01 Torr). Removal of the protective sheath of carbonyls by this method yields naked bimetallic nanoclusters which are highly active hydrogenation catalysts. The process of activation and the associated structural changes were principally followed by tempera-

0947-6539/98/0407-1216 $ 17.50+.50/0 *Chem. Eur. J.* **1998**, *4*, No. 7

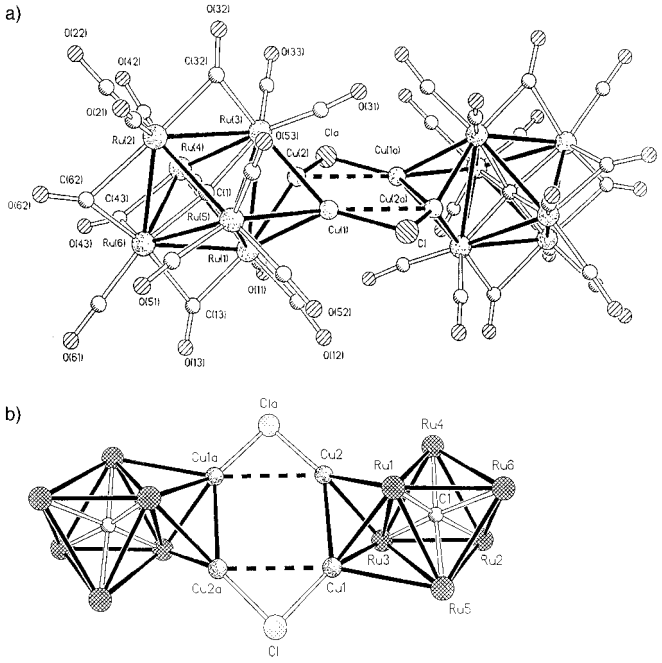

Figure 3. Molecular crystal structure diagram of the precursor carbonyl cluster anion $[Ru_{12}C_2(CO)_{32}Cu_4Cl_2]^{2-}$, a) including carbonyl ligands, b) excluding carbonyls.

ture-resolved in situ studies by means of FT-IR spectroscopy and X-ray absorption techniques (XANES and EXAFS) using near-identical treatment protocols. The results of these investigations are discussed below.

a) FT-IR spectroscopy: A pressed pellet was heated inside an evacuated, purpose-built FT-IR cell[35] and its IR spectra recorded at various temperatures. From the IR trace after heating for 2 h at 200 °C we can deduce that there are no carbonyl species remaining in the material. It is of interest to note that absorptions due to the phenyl stretching modes of the PPN cations (ca. 1440 cm^{-1}) may still be identified after heating at this temperature (vide infra). We can also see a significant rearrangement of the adsorbed species between 80 and 130 °C (as shown in the XANES Cu_K and Ru_K spectra, vide infra). It is tempting to suggest that this transition is the anchoring process of the bimetallic clusters, wherein Cl ligands on the Cu atoms are replaced by Si–O groups and the two Ru octohedra condense over the nascent copper raft. Futher examination over a range of higher temperatures then show these cluster condensates being slowly denuded of their CO sheath. The true nature of these carbonyl-deficient intermediates is difficult to determine. Indeed, the broad appearance of the CO stretching absorptions in the latter stages of the experiment suggests there are different species present in several stages of decarbonylation. Above 130 °C the terminal CO region displays a maximum at approximately 1974 cm^{-1}. This shows a shift to lower energy for the CO stretch as compared to the precursor and may indicate the electron-rich nature of the condensed bimetallic carbonyl cluster by increased $M\delta \rightarrow \pi^*$ donation (Dewer–Chatt–Duncanson model). During the final stages of decarbonylation of the metal particles the absence of μ_4-CO species, indicated by stretches at ca. 1430–1390 cm^{-1}, was surprising.[36] It would appear that these species need an extended surface or a step site to exist.[37]

b) X-ray absorption spectroscopy (XAS): A systematic in situ XAS investigation provided a great deal of information on the nature of the production of the bimetallic catalyst described here. The catalyst precursor was heated up to various temperatures prior to room-temperature XAS measurements. The results of these investigations are discussed below.

In the system under discussion, two edges (Ru K and Cu K) are accessible and complementary information can be obtained (Figure 4). The XANES region of the Cu K-edge (cf. Fig.4a) shows very clear changes upon thermolysis, the most

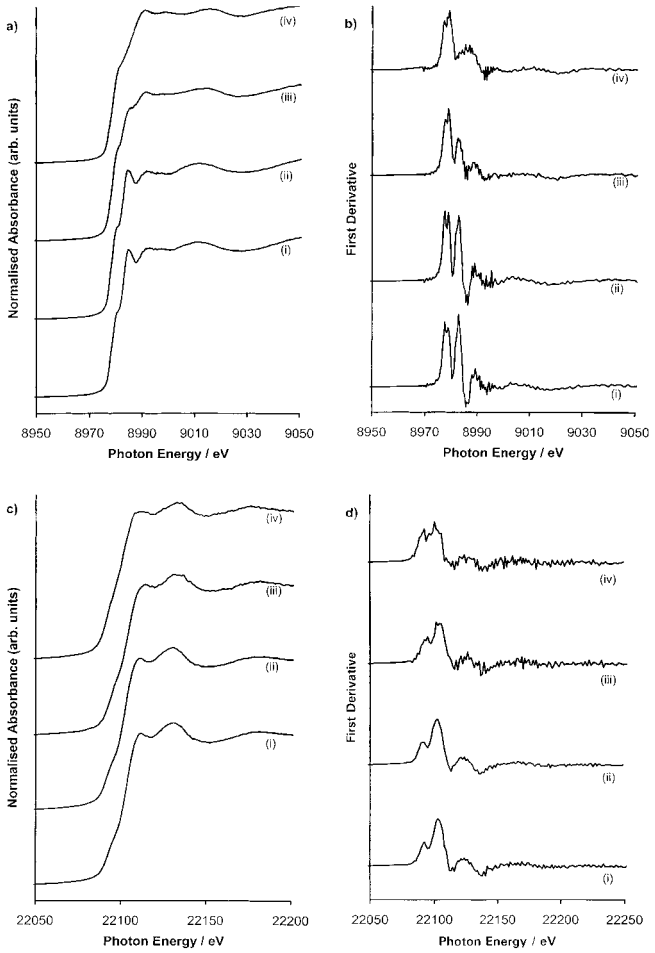

Figure 4. a) XANES spectra and b) first derivatives of Cu K-edge data and c) XANES spectra and d) first derivatives of Ru K-edge data taken during thermal activation, of i) catalyst as prepared, ii) heated to 80 °C, iii) heated to 130 °C and iv) heated to 180 °C.

striking feature being a gradual decrease of a peak in the near edge which is clearly seen in the first derivative shown in Figure 4b and results from changes in the types of near neighbours. However, the overall position of the absorption edge does not differ markedly, indicating no major changes in the electronic state of copper atoms. The XANES data of the Ru K-edge reveal only moderate changes upon heating. These modifications in the XANES region occur at temperatures as

low as 80 °C, possibly indicating alterations in the electronic structure due to changes in the local environment (which is more apparent in the EXAFS results) around the copper, owing to increasingly strong interactions with the surface silanols.

Examination of the changes in the associated Fourier transforms (shown in Figure 5) of the corresponding Ru K-edge EXAFS data corroborates the loss of carbonyls, revealing profound structural changes even at 80 °C (this is also borne out by the FT-IR studies, vide supra), culminating in the formation of the metal nanoparticle at 180 °C. Interestingly, the Cu K-edge EXAFS data suggest that its structural environment undergoes significant modification only between 130 °C and 180 °C (Figure 5). Although it is possible to analyse the EXAFS data recorded at various temperatures, our primary interest was to gain quantitative information on the final bimetallic cluster. This was achieved by a detailed analysis of the EXAFS data in terms of a structural model based on the structure of the precursor material. The analysis was relatively uncomplicated for the Ru K-edge; however, the Cu K-edge data proved intractable. Although it is possible to analyse the Cu K-edge EXAFS data by considering a Cu – O shell at approximately 1.9 Å and either Cu – Cu or Cu – Ru shell in the range of 2.5 to 2.65 Å, both the bond lengths and coordination numbers obtained after refinements were found to be considerably lower than what one would expect for either monometallic (if there is elemental/phase separation) or bimetallic Cu – Ru systems. This is likely to be caused by the presence of both types of neighbours (Cu and Ru) around the central Cu atom, a chemical postulate consistent with our previously reported study of Ag – Ru nanoparticles.[20] Hence, the reason for the low coordination number and chemically unreasonable bond lengths obtained when considering only one type of Cu – Cu or Cu – Ru neighbours can be found when examining the opposing nature of the EXAFS oscillations generated for these two scattering pairs. In Figure 6 we depict the EXAFS oscillations resulting from a Cu – Cu and Cu – Ru pair (Figure 6a,b) and from the addition of these two (Figure 6c,d), the last showing a marked decrease in amplitude due to phase cancellation.

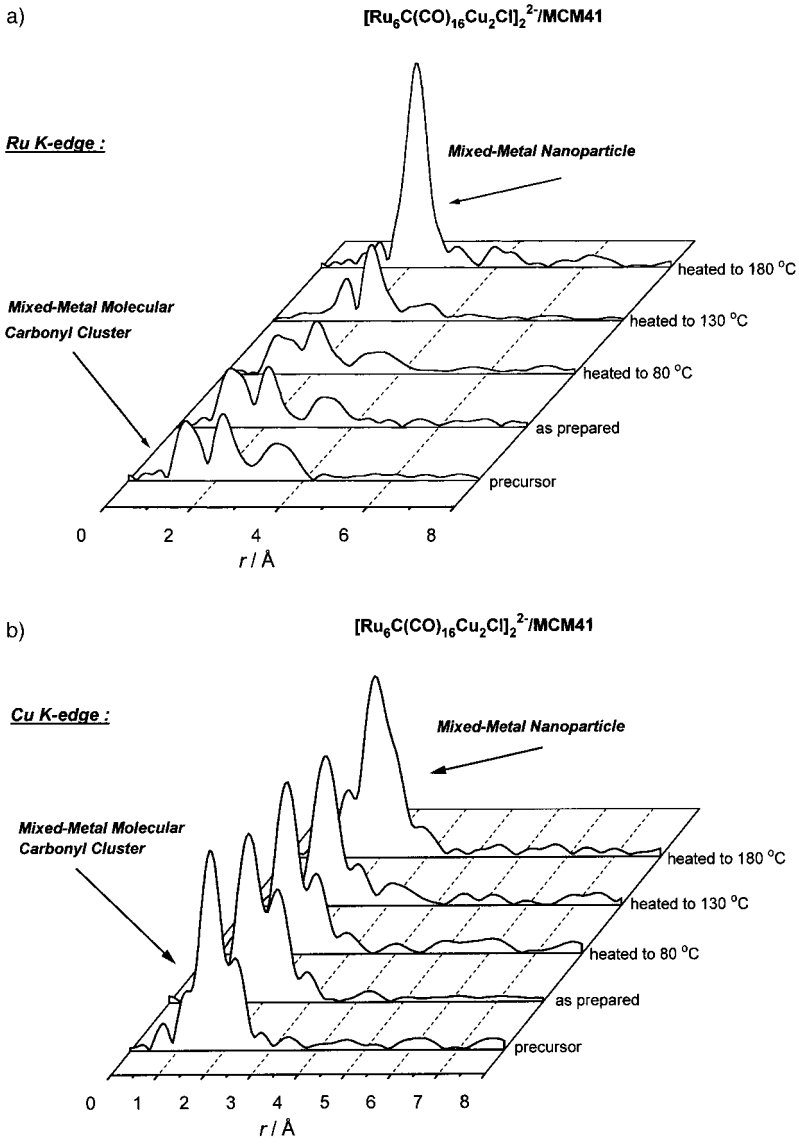

Figure 5. Fourier transforms of EXAFS data taken during thermal activation: a) Ru K-edge data, b) Cu K-edge data.

The detailed analysis of the data taking into account both Cu – Cu and Cu – Ru neighbours did indeed yield a superior fit compared with that obtained using a single Cu – Cu or Cu – Ru shell. The associated coordination numbers as well as bond lengths are found to be chemically much more sensible values, the model being comprised of coordination environments of 4.3 Ru at approximately 2.66 Å and 1.1 Cu at approximately 2.59 Å for the Ru K-edge data and 0.9 O at $\approx$1.95 Å, 3.1 Cu at $\approx$2.53 Å and 2.1 Ru at $\approx$2.59 Å for the Cu K-edge data (see Table 1), demonstrating the bimetallic nature of the particles. However, in the Cu K-edge data analysis the heavy scattering of the Ru atoms still dominated. To overcome potential problems with correlation effects, we made use of the recently developed strategy of analysing both the EXAFS data sets simultaneously. This methodology has several advantages; in particular, bond lengths of the two scattering pairs (in this case Cu – Ru from the Cu K-edge and Ru – Cu from the Ru K-edge) are refined together to achieve identical values and any distortions in the coordination numbers resulting from correlations between closely similar bond lengths can be resolved. The *simultaneous* refinement of both the data sets was performed using XFIT-(WIN 95) and one common local environment around both Cu and Ru atoms (see Figure 7 and Table 2 below).

In the model shown above, Cu(0) is an absorber surrounded by scatterers Ru(0), Ru(2), Cu(1) and O and Ru(0) is the other absorber, surrounded by Ru(1) and Cu(0). The refinement of the environment around either absorber is performed in turn, but taking account of both data sets simultaneously. This

0947-6539/98/0407-1218 $ 17.50+.50/0 *Chem. Eur. J.* **1998**, *4*, No. 7

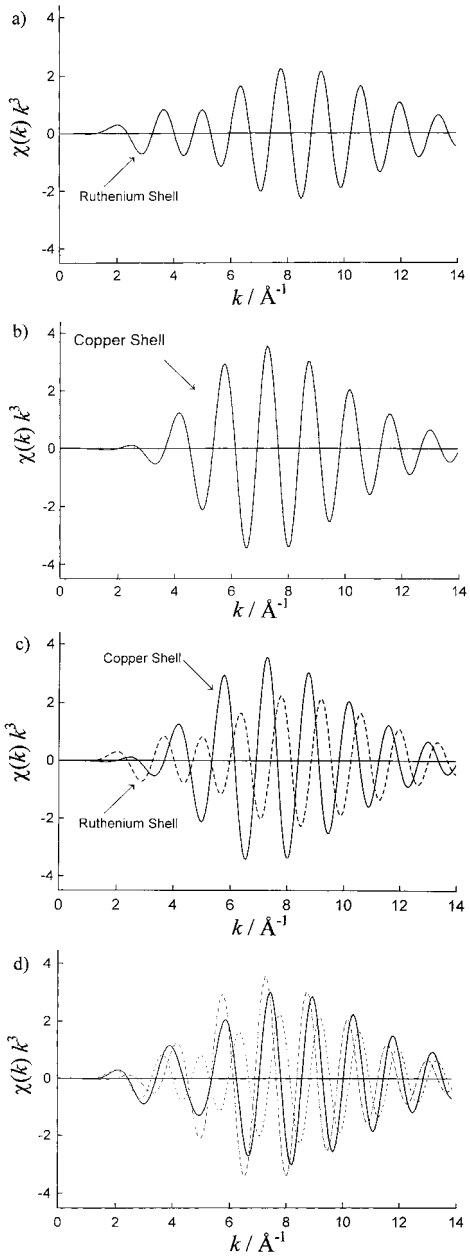

Figure 6. Figure 6. EXAFS simulations of single shells: a) ruthenium shell, b) copper shell, c) superposition of both shells and d) summation, solid line, and individual components, broken lines.

Table 1. Individual K-edge analysis.

Absorber	Scatterer	N	R [Å]	σ^2 [Å^2]	R factor [%][a]
Ru	Ru	4.3	2.66	0.005	23.27
	Cu	1.1	2.59	0.006	
Cu	O	0.9	1.95	0.012	12.69
	Cu	3.1	2.53	0.009	
	Ru	2.1	2.59	0.009	

[a] Reliability factor.

improves the ratio of data points to variables, and hence provides a more conservative approach. The shells were allowed to vary in terms of occupancy, Debye–Waller factor and absorber–scatterer distance. Several constraints and

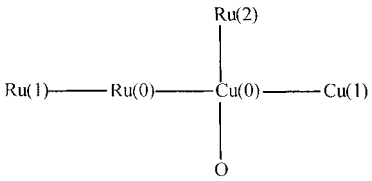

Figure 7. Structural model used in dual edge EXAFS data refinement, where Ru(0) and Cu(0) are the absorbers.

Table 2. Combined K-edge (Cu and Ru) refinement.

Absorber–scatterer	N	R [Å]	σ^2 [Å^2][a]	R factor
Ru(0)–Cu(0)	1.1	2.59	0.003	16%
Cu(0)–Cu(1)	2.7	2.54	0.003	
Cu(0)–Ru(0)	0.9	2.59	0.003	
Ru(0)–Ru(1)	3.9	2.66	0.003	
Cu(0)–O	1.4	1.97	0.006	
Cu(0)–Ru(2)	1.4	2.59	0.003	

[a] Held equal for all metals during refinement.

restrains were imposed, such as the Debye–Waller factors being set equal for Ru(0) and Ru(2) or setting shell occupancies to lie within the limits of between 1 ($\pm$1) to 8 ($\pm$1) to minimise any correlation effects between coordination numbers and Debye–Waller factors during the refinement process. The results obtained by using this approach (fits and raw data shown in Figure 8) demonstrate and confirm the bimetallic nature of the particles.

Scanning transmission electron microscopy (STEM) investigations: In order to evaluate the particle size and understand its morphology, we used a dedicated STEM (probe size $\approx$ 0.5 nm).[20] The key point with high annular dark-field imaging is that the intensity of the (Rutherford) scattered beams is directly proportional to Z^2, where Z is the atomic number of the scattering element. Thus, heavy atoms (such as Ru and Cu) stand out very clearly on a light background of Si and O. Analysis by energy dispersive X-ray emission (EDX) further confirmed the relative average atomic proportions of the bimetallic particles. Moreover, electron-stimulated X-ray maps further confirm the uniformity of the supported bimetallic nanoparticles (compare with the figures in ref. [20]).

Figure 9 shows the annular dark-field images from the Cu_4Ru_{12} bimetallic particles (EDX analysis yields a Ru:Cu ratio of 2.9) before and after an electron exposure of 12×10^{25} electrons m^{-2} respectively. In particular, Figure 9a presents a MCM41 cylindrical bundle of 4 channels across, curved at either end. Four distinct particles inside one of the channels have been marked. In Figure 9b the mesoporous structure of the MCM41 is vitrified owing to beam damage. However, the position of the 4 nanoparticles marked in the previous image has not changed and there is no sign of aggregation, in spite of the fact that they are very close to one another under an electron beam so intense as to destroy the structural integrity of the support. Comparison of the two images shows that this also holds for the other particles, thus further confirming the strength of the anchoring on the MCM41 surface of the Cu–Ru nanoparticles.

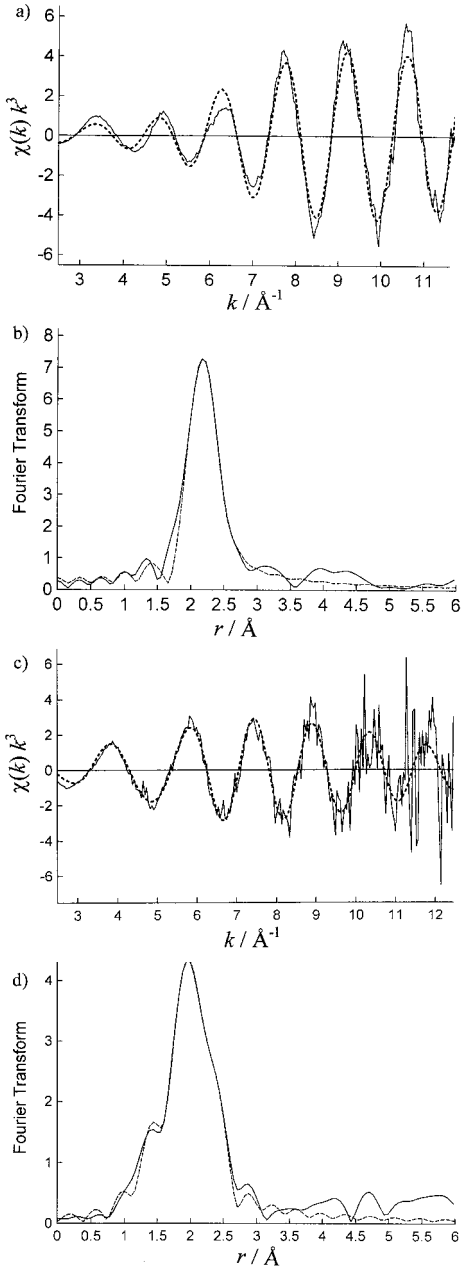

Figure 8. a) Cu K-edge EXAFS data, b) associated Fourier transform, c) Ru K-edge data, d) associated Fourier transform; solid lines experimental data, broken lines calculated spectra.

Figure 9c shows a histogram outlining the particle size distribution of the sample. The particle size is taken as the FWHM (full width half maximum) intensity in this image. Although this seems to be a widely used convention in particle size determination,[14] the particle intensities in the image are very much affected by the differences in defocus, especially so because of the narrow depth of field in the high-angle annular dark-field images. This means that the particles that are at different heights within the sample have different intensity distributions, that is, different FWHM values. The size of a particle in the image can be thought of as a convolution of the main probe intensity profile and the scattering potential of the particle (a function of Z^2 and density distribution within the particle).[38] The effect of the noise further complicates an

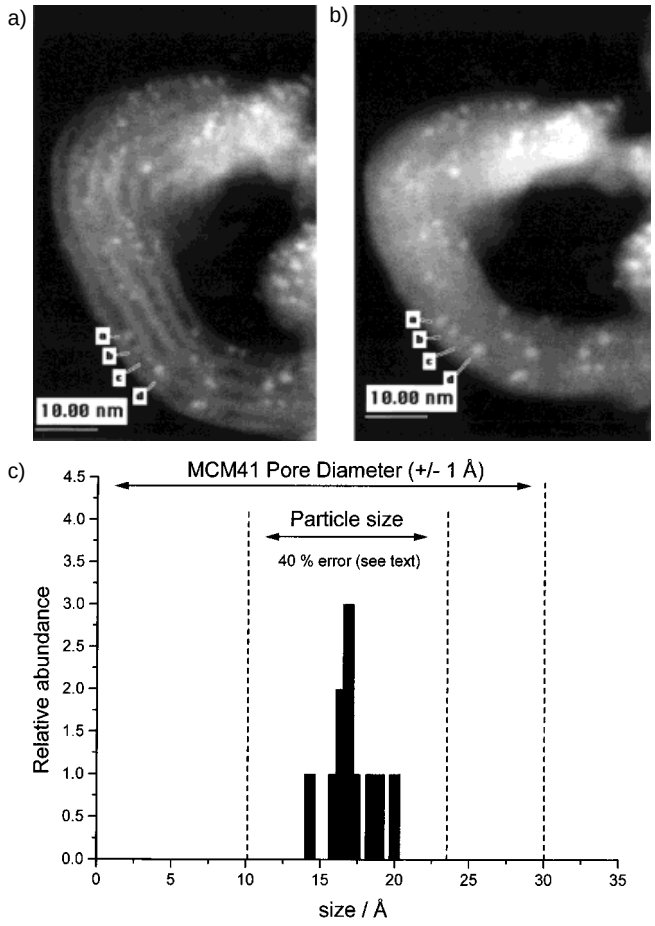

Figure 9. High-angle annular dark-field images of Cu_4Ru_{12} bimetallic particles inside MCM4 a) before and b) after vitrification due to electron beam damage; c) histogram of particle size distribution from image (a).

accurate determination. If a first approximate beam-broadening behaviour is considered (for a probe diameter of 5 Å and a beam convergence of 7 mrad on a 200 Å thick sample) the beam broadening is likely to increase the beam size by a minimum of 7.8 Å and the difference is more than 40 %, which is more than sufficient to explain the variations of FWHM in Figure 9c. An extensive discussion of these considerations has been previously published by Ozkaya et al.[39]

Thermogravimetric studies: To determine the weight loss on heating the sample under activation conditions, the bulk sample was heated and the weight loss recorded periodically, giving the results shown in Figure 10. The graph shows two regions of different but near-constant rates. The first [A to B] is believed to show the weight loss resulting from the carbonylate clusters and silanol condensation, whilst the second part [B to C] is due to silanol condensation alone. Extrapolation from BC to the ordinate gives the % weight loss excluding that due to siloxane formation (assuming the rate of this process is constant at low loading). The figure of 10.5 % thus obtained is entirely consistent with the weight loss due to complete decarbonylation of the cluster species, FT-IR and microanalysis [C, H, N, Cl]. Using this result we assumed that thermal activation for 2 hours at 190 °C gave a 11.5 % weight loss for the purposes of calculation of catalytic turnover frequencies (TOFs).

0947-6539/98/0407-1220 $ 17.50+.50/0 *Chem. Eur. J.* **1998**, *4*, No. 7

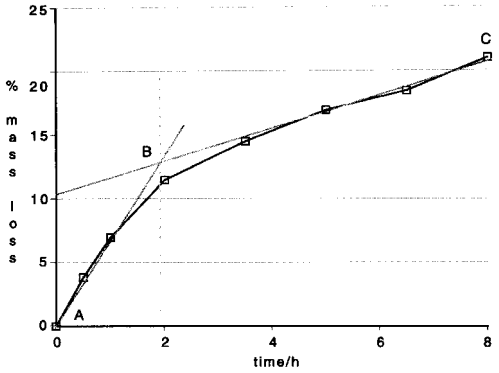

Figure 10. Graph used in the weight-loss extrapolation of gravimetric measurements.

Catalytic evaluation: The catalytic performance of the supported bimetallic nanoparticles in the hydrogenation of unsaturated molecules was tested on a wide variety of unsaturated species: hex-1-ene, phenylacetylene, diphenylacetylene, *trans*-stilbene, *cis*-cyclooctene and D-limonene. The highly efficient hydrogenation of hex-1-ene was accompanied by the isomerisation reaction to *cis*- and *trans*-hex-2-ene, which were subsequently hydrogenated (albeit at a much slower rate) as the reaction continued. Phenylacetylene is completely converted to ethylbenzene under the reaction conditions used. No hydrogenation of the phenyl group was detected. Hydrogenation of diphenylacetylene gave both stilbene (predominently *trans*-) and dibenzyl.[40]

Painstaking kinetic studies at 20 bar hydrogen and 373 °C show an induction time of 60 minutes and an overall turnover frequency of 25700 mol[hex] mol$[Cu_4Ru_{12}]^{-1}$ h^{-1}. The kinetic details are summarised in Figure 11. The observed induction time has several possible causes, for example in situ activation of the catalyst particles by further reduction in hydrogen, diffusion of hydrogen into the mesoporous structure, diffusion-induced lag of product emerging from the mesopores or effusion of PPNCl. These different aspects are currently being investigated by varying the silica support structure and by

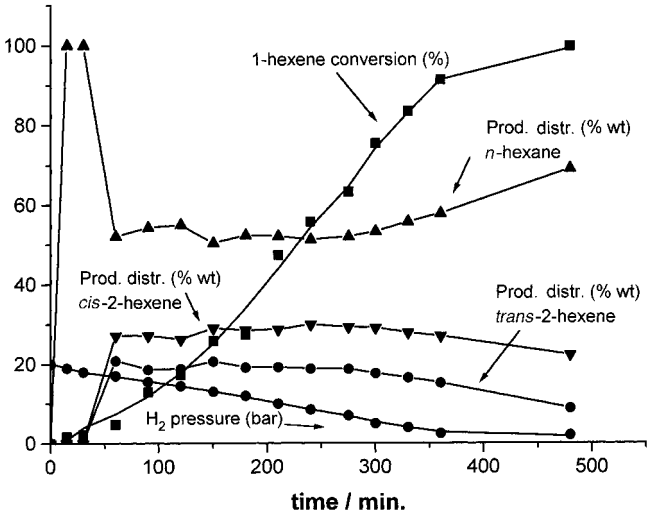

Figure 11. Plot of the hydrogenation of hex-1-ene at 20 bar versus time, showing total conversion, product distributions and hydrogen pressure variation (1-hexene: 44.7 g, $Ru_{12}Cu_4$/MCM-41: 20 mg, *T*: 373 K).

conducting competition experiments. The hex-1-ene conversion is practically linear with time after the initial induction period and the product distribution does not change significantly until after about 360 mins. Interestingly, although the major product (as expected) is *n*-hexane, significant amounts of *cis*- and *trans*-2-hexene are also formed, with the ratio of both isomers remaining constant around 1.5:1 for the major part of the reaction. The increase in selectivity for *n*-hexane after 480 mins, is probably a result of the subsequent hydrogenation of the *cis*- and *trans*-hex-2-ene isomers.

The hydrogenation of an internal olefin (*cis*-cyclooctene) was also studied at ambient temperature and H_2 pressure. Kinetic data obtained for this reaction (Figure 12) shows

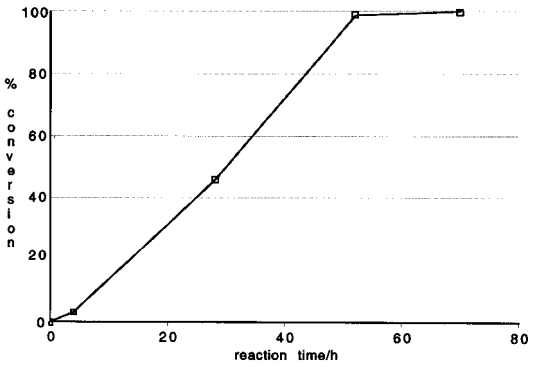

Figure 12. Plot of the hydrogenation of cyclooctene at 1 bar versus time, showing total conversion.

smooth conversion to cyclooctene. D-limonene, which contains both internal and pendant olefin groups, also readily underwent hydrogenation, and analysis of the final product mixture suggested a preference for hydrogen addition at the pendant olefin.[41] Little or no selectivity over the formation of *cis*/*trans*-1-methyl,4-isopropylcyclohexane (29% conversion to the *cis* and 34% conversion to *trans* isomer) could be observed. This perhaps mirrors the small size of the catalytically active species, in that double binding of the substrate might not be possible.

Discussion

The present study introduces a novel method of preparing bimetallic catalyst anchored to high-surface-area mesoporous silica (MCM41). The FTIR spectroscopic results identify the nature of the loss of carbonyl ligands associated with the thermal activation of the cluster. However, these results alone cannot provide further information about the nature of the final bimetallic cluster, and so we turned to the powerful combination of STEM, XANES and EXAFS studies. Qualitatively, both XANES and EXAFS results corroborate the IR results, in that there are substantial structural modifications during the thermolysis. The final detailed EXAFS data analysis of both the Ru and Cu K-edge data, in particular using the recently developed methodology of simultaneously refining both K-edge data sets, quantitatively revealed the presence of bimetallic clusters, with the Ru–Cu distance lying between those of bulk Ru–Ru and Cu–Cu.[42] Neither the

average Ru–Ru distances nor the Cu–Cu distances are significantly smaller (as one would expect for small metallic clusters) than that of twelvefold coordination in the bulk metal (although the low coordination numbers clearly suggest the presence of small particles, as does STEM). This is surprising, but may be explained by the cluster–surface interaction stretching the structure and/or by the presence of carbido atoms which would be undetectable by EXAFS. The argument that the carbido atom remains in the centre of the Ru octahedron is a strong one, as these structural fragments are chemically very stable and our activation conditions are very mild. Iwasawa and Izumi have reported[43] the contraction and expansion (inhaling and exhaling in the presence of CO) of Ru–Ru bond lengths (corresponding closely to our data) in ruthenium and rhodium clusters when deprived of, or exposed to, CO under conditions similar to those employed here. That there is anchoring of the bimetallic particle to the surface by the formation of Cu–O bonds is evident from the EXAFS results, since only one Cu–O shell is present and there is no direct indication for any Ru–O shells. Consistent with these results, we may construct a detailed structural picture of the nanoparticle, the principal characteristic of which is an exterior dome of twelve Ru atoms, linked by a base of four Cu atoms which are, in turn, covalently bonded to oxygens that, by inference, are themselves bound to the silicons of the support. Hence, we propose the model shown in Figure 13, derived from EXAFS and incorporating carbido atoms. On the basis of these arguments, we suggest that the

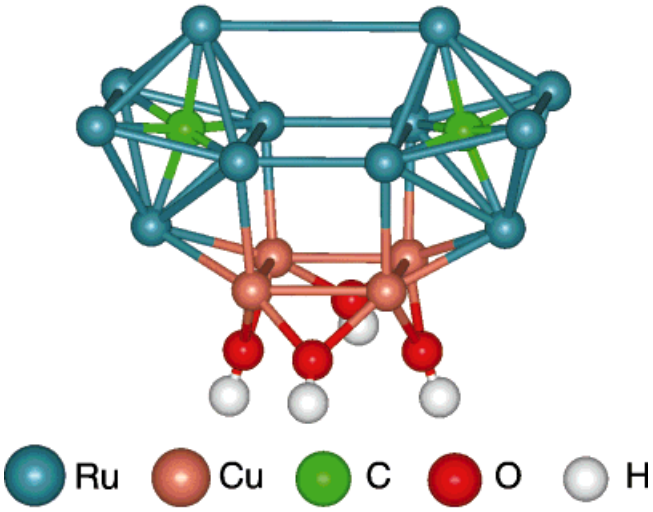

Figure 13. Energy-minimised model of naked metal particle attached to a silica surface, based on EXAFS analysis and on the breathing carbido model of Iwasawa and Izumi, showing the internal structure of the particle and the Van der Waals radii.

particle is very small ($\approx$14 Å diam.), indeed, too small to use EXAFS reliably to estimate its size. Further support for the proposed cluster geometry was provided by computer simulation: A model of the cluster consistent with the EXAFS data was subjected to an energy-minimisation calculation with the program Discover[44] and the *esff* forcefield. The minimised structure is shown in Figure 13. Additionally, using the minimised model it was possible to simulate a Cu and Ru K-edge EXAFS spectrum, the Fourier transform envelope of which was comparable to the experimentally observed ones in terms of shape and amplitude.

Annular dark-field electron microscopy is able to pinpoint the rather uniform spatial distribution of these particles, and establishes (as does the EXAFS analysis) that there is no fragmentation or sintering during catalysis, further rationalising the remarkable catalytic performance of these bimetallic nanoparticles. From a very careful and conservative analysis of our STEM images we estimate the maximum particle size to be around 23 Å when allowing for an error of +40%. Thus, the EXAFS structural model (being about 14 Å across), further refined by forcefield minimisations, would be perfectly consistent with the observeables and with general chemical considerations.

Together these results demonstrate that our initial strategy of removing the stabilising CO sheath from a mixed-metal cluster to produce a well-defined metal nanoparticle and anchoring the more oxophilic second metal to the MCM-41 surface has met with success**.** This work also reveals that there is abundant scope for further exploitation of bimetallic metal-cluster carbonylates as precursors for other supported nanoparticle catalysts. Moreover, a wide range of catalytic reactions besides hydrogenation awaits study.

Experimental Section

Materials and methods: All reactions were carried out under exclusion of air with solvents freshly distilled under an atmosphere of nitrogen or argon. Solution IR spectra were recorded on a Perkin–Elmer 1600 series FTIR in CH_2Cl_2 using NaCl cells or a Nujol mull. Negative fast-ion bombardment mass spectra were obtained on a Kratos MS 50 TC spectrometer with CsI as calibrant. Products were separated with Merck thin-layer chromatography (tlc) plates as supplied; 0.25 mm layer of Kieselgel 60 F254. $[Ru_3(CO)_{12}]$, $[Ru_6C(CO)_{16}][PPN]_2$ and MCM41 were prepared by the literature procedures.[27, 45, 46] CuCl was purchased from Aldrich and used without further purification.

Synthesis of $[Ru_{12}C_2Cu_4Cl_2(CO)_{32}][PPN]_2$: $[Ru_6C(CO)_{16}][PPN]_2$ (0.5 g) was refluxed in THF (20 mL) for 5 h with excess CuCl (1.0 g). The reaction mixture was cooled and filtered and an excess of PPNCl added. The solvent was then removed in vacuo and the mixture dissolved in CH_2Cl_2 and layered with ethanol to give deep red crystals. These were washed with ethanol and pentane to yield 385 mg of $[Ru_{12}C_2Cu_4Cl_2(CO)_{32}][PPN]_2$. Elemental analysis: 35.60% C, 1.74% H, 0.69% N, 6.89% Cu (calcd 35.9% C, 1.71% H, 0.79% N, 7.18% Cu); +FAB MS: $m/z = 2997$ $\{[Ru_{12}C_2Cu_4Cl_2(CO)_{32}][PPN]\}^-$, 2427 $\{[Ru_{12}C_2Cu_4Cl_2(CO)_{31}]^-\}$; IR: $\tilde{\nu}_{CO}$ = 2059(m), 2021(vs), 2967(sh), 1947(sh), 1855(w sh), 1829(br w) cm^{-1}.

Preparation of MCM41/$[Ru_{12}C_2Cu_4Cl_2(CO)_{32}][PPN]_2$: The mesoporous silica [MCM41] (120 mg) was dried under high vacuum (0.01 mmHg) at 473 K for 6 h, then washed with dry solvent and dried again under high vacuum at 473 K. It was then slurried with dry ether (30 mL) and the copper–ruthenium cluster salt $[Ru_{12}C_2Cu_4Cl_2(CO)_{32}][PPN]_2$ (50 mg cluster for 57 mg MCM41, i.e. 47.0% cluster salt by mass) along with CH_2Cl_2 (0.1 mL) at ambient temperature in darkness for 72 h. The resulting pink solid was washed with ether (10 mL) and dried under high vacuum (0.01 mmHg) at ambient temperature for 4 h. Elemental analysis gave 16.85% C, 2.63% H and 0.2% N (calcd 16.8% C, 0.4% H, 0.80% N). Spectroscopic data for MCM41/$[Ru_{12}C_2Cu_4Cl_2(CO)_{32}][PPN]_2$: IR (Nujol): $\tilde{\nu}_{CO}$ = 2058(s), 2011(vs),1997(vs), 1981(s), 1912(sh m), 1958(w), 1948(w), 1968(w br), 1835(m br), 1822(w br) cm^{-1}.

Determination of mass loss on catalyst activation by thermolysis of MCM41/$[Ru_{12}C_2Cu_4Cl_2(CO)_{32}][PPN]_2$: A precise quantity of the mesoporous silica loaded with the bimetallic cluster was placed into an Al-foil bucket of known mass, which was loosely crimp-sealed. This was then

0947-6539/98/0407-1222 $ 17.50+.50/0 *Chem. Eur. J.* **1998**, *4*, No. 7

heated in sand (453 K) to ensure even heat transfer under vacuum (0.01 mmHg) for several periods of time (see graph) and weighed at each interval after careful cleaning with an air brush. After a combined time of 12 h the sample did not exhibit any bands in the CO stretching region and was submitted to elemental analysis, which gave 15.76% C, 2.74% H and 0.2% N.

Catalyst activation: thermolysis of MCM41/$[Ru_{12}C_2Cu_4Cl_2(CO)_{32}][PPN]_2$: A precise quantity of MCM41/$[Ru_{12}C_2Cu_4Cl_2(CO)_{32}][PPN]_2$ was loaded into an Al-foil bucket inside an argon-filled Schlenk tube. The ensemble was then heated for 2 h at 453 K under vacuum (0.01 mmHg), after which the apparatus was purged with Ar or H_2 and the cooled catalyst transfered to the reaction vessel.

Hydrogenation of hex-1-ene (batch expt.): A 150 mL teflon-lined autoclave equipped with a magnetic stirrer was charged with catalyst ($\approx$8 mg), hex-1-ene (3.0 mL) and H_2 (64 bar). The ensemble was heated to 373 K for 4 h, after which the vessel was cooled to ambient temperature and the contents analysed by ^{1}H NMR to reveal $\geq$99% conversion to *n*-hexane.

Hydrogenation of hex-1-ene (kinetic study): A 150 mL PEEK-lined autoclave equipped with a magnetic stirrer was charged with catalyst (10 mg), hex-1-ene (44.6 g, 66.27 mL) and H_2 (20 bar). The ensemble was maintained at 373 K for 16 h, after which it was cooled to ambient temperature. Every 30 min samples were taken at high pressure and analysed by GC. A typical mass balance shows minimal sample loss: moles of 1-hexene taken: 0.532, product analysis: moles of *n*-hexane formed: 0.367, moles of *cis*-2-hexene formed: 0.122, moles of *trans*-2-hexene formed: 0.039, moles of 1-hexene remaining: 0.002, total moles of products: 0.530, loss (moles): 0.002, loss (grams): 0.168 g, loss (%): 0.4%.

Hydrogenation of diphenylacetylene: A 150 mL teflon-lined autoclave equipped with a magnetic stirrer was charged with of catalyst (7.1 mg), diphenylacetylene (400 mg), ethanol (1 mL), pentane (10 mL) and H_2 (65 atm). The ensemble was heated to 393 K for 6 d, after which the vessel was cooled to ambient temperature and the contents analysed by ^{1}H NMR and GC/MS to reveal 66% conversion to *trans*-stilbene, >0.5% conversion to *cis*-stilbene and 33% conversion to dibenzyl. >0.5% of unconverted starting material was detected. From these results an overall TOF_{hydro} of 16.8 mol[DPA] mol$[Cu_4Ru_{12}]^{-1}$ h^{-1} was calculated.

Hydrogenation of phenylacetylene: A 150 mL teflon-lined autoclave equipped with a magnetic stirrer was charged with catalyst (12.0 mg), phenylacetylene (1 mL), pentane (5 mL) and H_2 (65 atm). The ensemble was heated to 373 K for 24 h, after which the vessel was cooled to ambient temperature and the contents analysed by ^{1}H NMR and GC/MS to reveal $\geq$99.9% conversion to ethylbenzene; no unconverted starting material was detected. From these results an overall TOF_{hydro} of 615 mol[PA] mol$[Cu_4Ru_{12}]^{-1}$ h^{-1} was calculated (assuming styrene is the intermediate).

Hydrogenation of *trans*-stilbene: A 150 mL teflon-lined autoclave equipped with a magnetic stirrer was charged with catalyst (8.0 mg), *trans*-stilbene (400 mg), pentane (10 mL), ethanol (1 mL) and H_2 (65 atm). The ensemble was heated to 393 K for 48 h, after which the vessel was cooled to ambient temperature and the contents analysed by ^{1}H NMR and GC/MS to reveal 79% conversion to dibenzyl. 21% of unconverted starting material was detected. From these results an overall TOF_{hydro} of 69.5 mol[stil] mol$[Cu_4Ru_{12}]^{-1}$ h^{-1} was calculated.

Hydrogenation of *cis*-cyclooctene: A 250 mL Erlenmeyer flask equipped with a magnetic stirrer was charged with catalyst ($\approx$10 mg), *cis*-cyclooctene (10 mL) and H_2 (1 atm). The ensemble was kept at 298 K for 72 h, during which time the contents were analysed by ^{1}H NMR and GC/MS to reveal a steady conversion to cyclooctane. No unconverted starting material was detected after 72 h. From these results an overall TOF_{hydro} of 152 mol[cyclo-C8] mol$[Cu_4Ru_{12}]^{-1}$ h^{-1} was calculated.

Hydrogenation of D-limonene: A 150 mL teflon-lined autoclave equipped with a magnetic stirrer was charged with 13.0 mg of catalyst, D-limonene (1 mL) and H_2 (65 atm). The ensemble was heated to 393 K for 23 h, after which it was cooled to ambient temperature and the contents analysed by ^{1}H NMR and GC/MS to reveal 29% conversion to *cis*-1-methyl-4-isopropylcyclohexane, 34% conversion to *trans*-1-methyl-4-isopropylcyclohexane, >0.5% conversion to 1-methyl-4-isopropenylcyclohexane and 35% conversion to 1-methyl-4-isopropylcyclohex-1-ene. >1% unreacted starting material was detected. From these results an overall TOF_{hydro} of 362 mol[D-lim] mol$[Cu_4Ru_{12}]^{-1}$ h^{-1} was calculated.

EXAFS data collection and refinement: EXAFS data were recorded at the Daresbury SRS facility on station 9.2. The station was equipped with a Si(220) monochromator, and data were collected in fluorescence mode using a thirteen-element Canberra fluorescence detector. A powdered sample of each catalyst studied was pressed into a self-supporting wafer, and mounted in a custom-built in situ cell.[47] The EXAFS data were subsequently analysed with the XFIT (for Windows 95)[48] suite of programs. In the double-edge refinement the S_0^2 parameters were taken from the single-edge refinements and held constant and the σ^2 parameters were constrained to be equal for the copper and ruthenium atoms. Two E_0 parameters were included in the model, one for copper and one for ruthenium. All parameters (i.e. coordination numbers, distances, E_0 and σ^2 values) were refined simultaneously. The precise fitting protocol and theoretical underpinning will be published elsewhere.

High-resolution electron microscopy (HREM): Experiments were conducted with a field emission gun dedicated scanning transmission electron microscope (VG HB501) with a windowless EDX detector. MCM41 samples were prepared by crushing the particles between two glass slides and spreading them on a perforated carbon film supported on a Ti grid. The samples were briefly heated under a light bulb in the specimen preparation chamber of the STEM prior to their introduction into the microscope.

Acknowledgements: We thank the EPSRC for a rolling grant to JMT and a regular one to BFGJ, the EU for support of TM, and the Comissioners of the 1851 Royal Exhibition for an award to RR. GS was funded partly by JMT's rolling grant and the CCRL Daresbury Laboratory, to whom we are grateful.

Received: October 29, 1997 [F869]

[1] J. S. Beck, J. C. Vartuli, *Curr. Opin. Solid-State Mat. Sci.* **1996**, *1*, 76.
[2] J. M. Thomas, C. R. A. Catlow, R. G. Bell, in *Handbook of Heterogeneous Catalysis* (Eds.: G. Ertl, H. Koezinger, J. Weitkamp), VCH, Weinheim, **1997**.
[3] J. M. Thomas, W. J. Thomas, *Principles and Practices of Heterogeneous Catalysis*, Ch. 5, VCH, Weinheim, **1997**.
[4] J. Klinowski, J. M. Thomas, M. Audier, S. Vasudevan, C. A. Fyfe and J. S. Hartman, *J. Chem. Soc. Chem. Commun.* **1981**, 570.
[5] K. J. Balkus, A. Khanmamedova, A. G. Gabrielov, S. I. Zones, *Stud. Surf. Sci. Catal.* **1996**, *101*, 1341.
[6] R. F. Lobo, M. Tsapatsis, C. C. Freyhardt, S. Khodabandeh, P. Wagner, C. Y. Chen, K. J. Balkus, S. I. Zones, M. E. Davis, *J. Am. Chem. Soc.* **1997**, *119*, 8474.
[7] P. A. Wright, R. H. Jones, S. Natarajan, R. G. Bell, J. Chen, M. B. Hursthouse, J. M. Thomas, *J. Chem. Soc. Chem. Commun.* **1993**, 633.
[8] G. W. Noble, P. A. Wright, P. Lightfoot, R. E. Norris, K. J. Hudson, A. Krick, H. Graafsma, *Angew. Chem.* **1997**, *109*, 76; *Angew. Chem. Int. Ed. Engl.* **1997**, *36*, 81.
[9] T. Maschmeyer, F. Rey, G. Sankar, J. M. Thomas, *Nature (London)* **1995**, *32*, 696.
[10] J. M. Thomas, *Chem. Eur. J.* **1997**, *3*, 1557.
[11] R. D. Oldroyd, J. M. Thomas, G. Sankar, *Chem. Commun.* **1997**, *21*, 2025.
[12] J. H. Sinfelt, *Bimetallic Catalysts*, Wiley, New York, **1983**.
[13] J. H. Sinfelt, *Int. Rev. Phys. Chem*. **1988**, *7*, 281.
[14] M. S. Nasher, A. I. Frenkel, D. L. Adler, J. R. Shapley, R. G. Nuzzo, *J. Am. Chem. Soc.* **1997**, *119*, 7760.
[15] M. Ichikawa, *Adv. Catal.* **1992**, *38*, 283.
[16] B. C. Gates, *Chem. Rev.* **1995**, *95*, 511.
[17] O. Alexeev, M. Shelef, B. C. Gates, *J. Catal.* **1996**, *164*, 1, and references therein.
[18] J. M. Basset, J. P. Candy, A. Choplin, B. Didillon, F. Quigrard, A. Theolier, in *Perspectives in Catalysis* (Eds.: J. M. Thomas, K. I. Zamaraev), Blackwells/IUPAC, Oxford, **1992**, pp. 125–146.
[19] M. S. Nasher, D. M. Sommerville, P. D. Lane, D. L. Adler, J. R. Shapley, R. G. Nuzzo, *J. Am. Chem. Soc.* **1996**, *118*, 12964.
[20] D. S. Shephard, T. Maschmeyer, B. F. G. Johnson, J. M. Thomas, G. Sankar, D. Ozkaya, W. Zhou, R. D. Oldroyd, *Angew. Chem.* **1997**, *109*, 2337; *Angew. Chem. Int. Ed. Engl.* **1997**, *36*, 2242.

[21] M. S. Nasher, A. I. Frenkel, D. L. Adler, J. R. Shapley, R. G. Nuzzo, *J. Am. Chem. Soc.* **1997,** *119*, 7760.
[22] J. W. Couves, J. M. Thomas, G. N. Greaves, R. H. Jones, A. J. Dent, G. E. Derbyshire, *Nature (London)*, **1991**, *354*, 465.
[23] J. M. Thomas, G. N. Greaves, *Science*, **1994**, *265*, 1675.
[24] M. A. Beswick, Ph.D Thesis, University of Cambridge, **1992**, and references therein; M. A. Beswick, J. Lewis, P. R. Raithby, M. C. Ramirez de Arellano, *Angew. Chem.* **1997**, *109*, 303; *Angew. Chem. Int. Ed. Engl.* **1997**, *36*, 291.
[25] S. J. Taverner, J. H. Clark, G. W. Gray, P. A. Heath, D. J. Macquarrie, *J. Chem. Soc. Chem. Commun.* **1997**, 1073.
[26] J. S. Beck, J. C. Vartuli, W. J. Roth, M. E. Leonowicz, C. T. Kresge, K. D. Schmitt, C. T.-W. Chu, D. H. Olsen, E. W. Sheppard, S. B. McCullen, J. B. Higgins, D. L. Schlenker, *J. Am. Chem. Soc.* **1992**, *114*, 10834.
[27] F. Rey, G. Sankar, T. Maschmeyer, J. M. Thomas, R. G. Bell, G. N. Greaves, *Top. Catal.* **1996**, *3*, 121 – 126.
[28] D. Ozkaya, J. M. Thomas, W. Zhou, unpublished results.
[29] I. J. Shannon, J. M. Thomas, G. Sankar, T. Maschmeyer, M. Sheehy, D. Madil, R. D. Oldroyd, *Catal. Lett.* **1997**, *44*, 23.
[30] G. Sankar, P. A. Wright, S. Natarajan, J. M. Thomas, G. N. Greaves, A. J. Dent, B. R. Robson, C. A.Ramsdale, R. H. Jones, *J. Phys. Chem.* **1993**, *97*, 9550.
[31] J. M. Thomas, P. A. Wright, J. Chen, G. Sankar, G. N. Greaves, A. J. Dent, L. Marchese, *Angew. Chem.* **1994**, *106*, 1922; *Angew. Chem. Int. Ed. Engl.* **1994**, *33*, 1871.
[32] J. M. Thomas, *Faraday Disc. Chem. Soc.* **1996**, *105*, 1.
[33] M. A. Beswick, J. Lewis, P. R. Raithby, M. C. R. Dearellano, *J. Chem. Soc. Dalton Trans.* **1996**, *21*, 4033.
[34] Solvent extraction of this material with dichloromethane showed the bimetallic clusters can be quantitatively desorbed and remain chemically unchanged.
[35] G. Sankar, J. M. Thomas, C. R. A. Catlow, J. Turner, W. I. F. David, *Top. Catal.*, submitted.
[36] D. B. Brown, P. J. Dyson, B. F. G. Johnson, C. M. Martin, D. G. Parker, S. Parsons, *J. Chem. Soc. Dalton Trans.* **1997**, 1909.
[37] M. L. Colaianni, J. G. Chen, W. H. Weinberg, J. T. Yates, *J. Am. Chem. Soc.* **1992**, *114*, 3735.
[38] M. M. J. Treacy, S. B. Rice, *J. Microscopy* **1989**, *15*, 211.
[39] D. Ozkaya, J. M. Thomas, D. S. Shephard, T. Maschmeyer, B. F. G. Johnson, G. Sankar, R. D. Oldroyd, *Inst. Phys. Conf. Ser.* **1997**, *153(9)*, 403.
[40] The overall TOF of this reaction was unexpectedly low; this may be a result of deactivation by long-lived intermediates blocking reactive sites on the bimetallic particles. We are currently attempting to determine the cause of this loss of activity.
[41] The degree of substitution of a given olefin is known to be geometrically inversely proportional to the rate at which it may be hydrogenated on a metal surface; see *Comprehensive Organic Synthesis, Vol X*, Pergamon, Oxford, **1988**.
[42] The precise theoretical treatment of this approach for these systems will be published elsewhere, but is already available in its general form from the XFIT documentation, Australian Synchrotron Research Program, c/- ANSTO, Private Mail Bag 1, Menai, NSW, 2234 (Australia).
[43] V. Izumi, Y. Iwasawa, *ChemTech*, **1994**, 20.
[44] Discover 4.0.0, Molecular Simulations, San Diego, **1996**.
[45] J. N. Nicholls, M. D. Vargas, J. Hriljac, M. Sailor, *Inorg. Synth.* **1989**, *28*, 280.
[46] A. A. Bhattacharyya, C. C. Nagel, S. G. Shore, *Organometallics* **1983**, *2*, 1187.
[47] G. Sankar, J. M. Thomas, J. Chen, P. A. Wright, P. A. Barrett, G. N. Greaves, C. R. A. Catlow, *J. Nucl. Inst. Methods B* **1998**, *97*, 37 – 40.
[48] XFIT (for Windows 95), P. J. Ellis, H. C.Freeman, *J. Synchroton Radiat.* **1995**, *2*, 190.

  0947-6539/98/0407-1224 $ 17.50+.50/0